J Supercond Nov Magn (2013) 26:101–109
DOI 10.1007/s10948-012-1719-6

ORIGINAL PAPER

Analysis of Indentation Size Effect on Mechanical Properties of Cu-Diffused Bulk MgB_2 Superconductor Using Experimental and Different Theoretical Models

M. Dogruer · G. Yildirim · O. Ozturk · C. Terzioglu

Received: 26 June 2012 / Accepted: 2 July 2012 / Published online: 20 July 2012

Abstract This study indicates the change of the electrical, microstructural, physical, mechanical and superconducting properties of Cu-diffused bulk MgB_2 superconductors by means of scanning electron microscopy (SEM), X-ray diffraction analysis (XRD), microhardness and dc resistivity measurements. The samples are prepared at different annealing temperatures in the range from 650 to 850 °C. Electrical and superconducting properties of samples are estimated from the dc electrical resistivity measurements. Moreover, microhardness measurements are performed to investigate the mechanical properties. Further, phase composition, grain sizes and lattice parameters are determined from the XRD measurements. At the same time, the surface morphology and grain connectivity of the samples are examined by SEM investigations. The measurements conducted demonstrate that both the Cu diffusion into the MgB_2 system and the increment in the diffusion-annealing temperature increase the critical transition temperatures. Similarly, microstructure and grain size improve while the voids and porosity decrease with the increase of the diffusion-annealing temperature. In addition, the experimental results of the microhardness measurements are investigated using the Meyer's law, PSR (proportional specimen resistance), modified PRS (MPSR), elastic-plastic deformation model (EPD) and Hays–Kendall (HK) approach. The obtained microhardness values of the samples decrease with the increase of the diffusion-annealing temperature up to 850 °C. The Hays–Kendall approach is found to be the most successful model describing the mechanical properties of the samples studied in this work.

Keywords Cu-diffused bulk MgB_2 superconductors · Indentation size effect · Vickers microhardness · Meyer's law · PSR · MPSR · EPD · HK approach

1 Introduction

Mechanical properties of high-temperature superconductors are related to their physical properties. There are several models to predict the mechanical properties of materials. Among the different experimental methods, Vickers microhardness testing is a useful technique to evaluate the mechanical properties of solids in the form of bulk samples [1]. Ozturk et al. [2] investigated the mechanical and superconducting properties of iron diffusion-doped $Bi_{1.8}Pb_{0.35}Sr_{1.9}Ca_{2.1}Cu_3O_y$ superconductors and observed that the value of microhardness changed from 0.672 to 0.359 GPa in the applied load range of 0.245–2.940 N. The effect of Gd addition on the mechanical (microhardness, Young's modulus, yield strength and fracture toughness) properties of $Bi_{1.8}Pb_{0.35}Sr_{1.9}Ca_{2.1}Cu_3Gd_xO_{10-\delta}$, was also studied by Aydin et al. [3]. A decrease in the mechanical properties was observed as a consequence of the increment in the voids, porosity and weak links between the superconducting grains. Terzioglu [4] also carried out the investigation of the physical properties of $Bi_{1.8}Pb_{0.35}Sr_{1.9}Ca_{2.1}Cu_3Gd_xO_y$ superconductors. It was pronounced that the Meyer number (examining the sample exhibits Indentation Size Effect or Reverse Indentation Size Effect) increases when Gd content is increased.

M. Dogruer (✉) · G. Yildirim · C. Terzioglu
Department of Physics, Abant Izzet Baysal University, Bolu, 14280, Turkey
e-mail: musadogruer8@gmail.com

O. Ozturk
Department of Physics, Kastamonu University, Kastamonu, 37100, Turkey

On the other hand, the results obtained indicated that Kick's law is not valid because of the fact that Meyer number is found to be less than 2. In other words, the $Bi_{1.8}Pb_{0.35}Sr_{1.9}Ca_{2.1}Cu_3Gd_xO_y$ samples studied exhibited Indentation Size Effect (*ISE*). As is well known, the microhardness measurements of the materials depend sensitively on the applied load. If the microhardness value of a material decreases with the increase in the applied load, the behavior of the material undergoes *ISE* (Indentation Size Effect). Another case is defined as *RISE* (Reverse Indentation Size Effect), when the microhardness increases with the applied load. In this study, the effect of Cu diffusion on the mechanical properties of MgB_2 superconductor materials is examined by Vickers microhardness measurements and it is found that the Cu-diffused bulk MgB_2 samples exhibit the *ISE* behavior. The results of the microhardness measurements are analyzed employing various methods such as Meyer's law, Hays–Kendall approach, PSR, MPSR and EDP models. HK approach is found to be the best model defining the microhardness of the Cu-diffused bulk MgB_2 superconductors. Additionally, dc electrical resistivity measurements for electrical and superconducting properties; SEM analyses for surface morphology and grain connectivity; and XRD measurements for the phase composition, grain sizes and lattice parameters of the samples are conducted. The results obtained show that both the Cu diffusion into the system and the increment in the diffusion-annealing temperature improve the superconducting, microstructural, physical, and especially mechanical properties of the samples prepared.

2 Experimental Techniques

The starting material in this work is commercially available powder of MgB_2 (obtained from Alfa Aesar, -325 mesh, >44 micron). The precursor powder is filled into rectangular bars of $40 \times 4 \times 2$ mm^3 in high purity argon (Ar) gas atmosphere inside a glove box and pressed by applying a load of 350 MPa at room temperature. After the pelletization process, the weight of each bar obtained is about 0.25 g. Then, the bulk samples wrapped with Ta foil are placed into quartz tube for annealing process. The bars are annealed in the tube furnace (Protherm-Model PTF12/75/200) with 5 °C/min heating rate at 850 °C for 1 h under 5 bar high purity argon gas atmosphere. The bars sintered are left in the furnace to cool down to approximately room temperature. Additionally, on one face of the samples the Cu evaporation (thickness of about 30 μm) is performed using an AUTO 306 vacuum coater (EDWARDS) under pressure of 2×10^{-5} Torr. At the end of the evaporation process, it is controlled by attaching the Cu layer to the samples prepared by visual inspection and the mechanical damage method via a razor blade. Finally, the Cu evaporated superconducting samples are sintered at 650, 700, 750, 800 and 850 °C for 1 h. In the current work, the undiffused sample is denoted as Cu-0 while the Cu diffused MgB_2 superconductors produced by various annealing temperature such as 650, 700, 750, 800 and 850 °C will hereafter be denoted as Cu-650, Cu-700, Cu-750, Cu-800 and Cu-850, respectively.

The dc resistivity is measured as a function of temperature in the range of 30–45 K for the prepared samples by using the standard four-point probe method by a closed-cycle cryostat at low temperatures down to 3 K. A constant dc current of 5 mA is introduced between the contacts covered with silver paint to minimize the contact resistivity. A Keithley 220 programmable current source and a Keithley 2182A nano-voltmeter are used for the resistivity measurements. Moreover, where the resistivity begins to decrease significantly a temperature value is defined as the onset critical temperature (T_c^{onset}) of the sample, while the offset transition temperature (T_c^{offset}) is determined as the temperature at which $R = 0\ \Omega$.

At the same time, X-ray diffraction measurements are carried out using a Rigaku Multiflex + XRD diffractometer with CuK_α target giving a monochromatic beam with 1.5418-Å wavelength in the range $2\theta = 3$–$60°$ at a scan speed of $3°$/min and step increment of $0.02°$ at room temperature (300 K). The lattice parameters, phase structures and impurities in the samples are obtained from the XRD patterns. The accuracy in determining the lattice parameters (a and c) is found to be ± 0.0001 Å. Additionally, the average particle sizes of the samples prepared are computed using the Scherrer–Warren approach.

Further, the grain connectivity and surface morphology of the samples are investigated using a Jeol scanning electron microscope (SEM) JEOL 6390-LV, operated at 20 kV, with a resolution power of 3 nm.

Besides, Vickers microhardness measurements are conducted at room temperature in air by using a digital microhardness tester (SHIMADZU HVM-2) to obtain information about the physical and mechanical properties of the bulk MgB_2 samples annealed at different temperatures. A rigid Vickers pyramidal indenter is applied for 10 s using different load in the range from 0.245 to 2.940 N and the diagonals of indentation are measured with an accuracy of ± 0.1 μm. The Vickers microhardness measurements are performed with an average of 20 readings at different locations of specimen surfaces to obtain reasonable mean values for each applied load. The microhardness measurements are examined by means of the various models such as Meyer's law, proportional specimen resistance (PSR), modified PRS (MPSR), elastic-plastic deformation model (EPD) and Hays–Kendall (HK) approach.

Table 1 Some characteristics of superconducting samples

Samples	T_c^{onset} (K)	T_c^{offset} (K)	ΔT_c (K)	$\rho_{300\ K}$ (μΩ cm)	a (Å)	c (Å)	Grain size (nm)
Cu-0	38.4	36.9	1.5	62	3.0831	3.5193	55
Cu-650	38.6	37.2	1.4	58	3.0846	3.5269	58
Cu-700	38.8	37.5	1.3	86	3.0857	3.5274	63
Cu-750	39.1	37.9	1.2	107	3.0862	3.5279	68
Cu-800	39.2	38.1	1.1	115	3.0882	3.5284	71
Cu-850	39.3	38.3	1.0	129	3.0886	3.5345	74

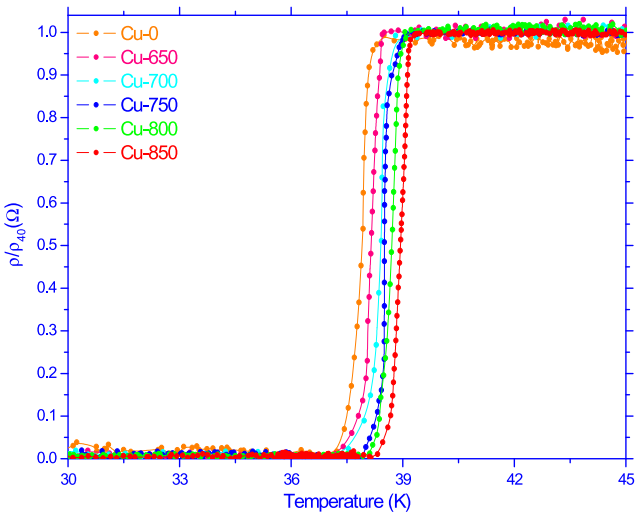

Fig. 1 Normalized resistivity as a function of temperature curves for Cu-0, Cu-650, Cu-700, Cu-750, Cu-800 and Cu-850

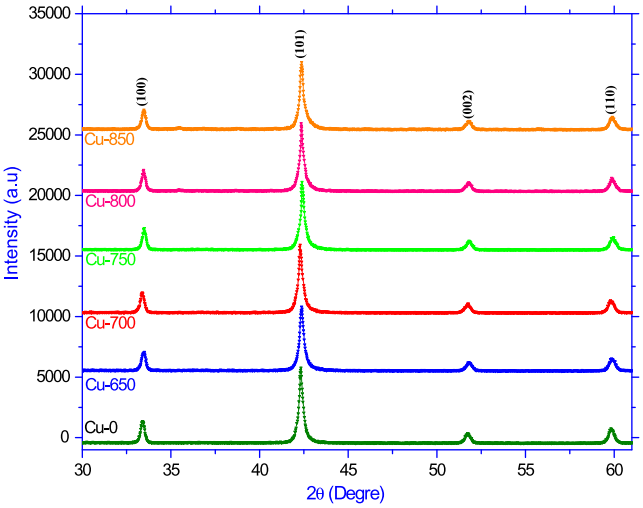

Fig. 2 XRD patterns of Cu-0, Cu-650, Cu-700, Cu-750, Cu-800 and Cu-850 samples

3 Results and Discussion

3.1 Electrical Resistivity Measurements

Table 1 indicates the room-temperature resistivity determined from I–V curves of the samples. It is obvious from the table that the resistivity increases systematically with the increase of the diffusion-annealing temperature to a maximum (129 μΩ cm) for the Cu-850 sample as against 58 μΩ cm for the Cu-650 sample. The electrical resistivity is measured using the standard four-probe dc method in the temperature range from 30 to 45 K. Moreover, the normalized resistivity graphs of the samples are given in Fig. 1. As seen from the figure, all the samples exhibit the metallic behavior in the normal state. The onset (T_c^{onset}) and offset (T_c^{offset}) critical temperature values deduced from the normalized resistivity graphs are also tabulated in Table 1. It is visible from the table that the offset and onset critical temperatures of the samples analyzed in this work are observed to be in the range of 38.3–36.9 K and 39.3–38.4 K, respectively. All the results obtained show that both T_c^{onset} and T_c^{offset} values regularly increase with the increase of the diffusion-annealing temperature up to 850 °C. At the same time, the variation of temperature, ΔT_c ($T_c^{onset} - T_c^{offset}$), is demonstrated in Table 1. It is seen that ΔT_c decreases with the increase of the annealing temperature. When the ΔT_c is observed to be about 1.5 K for a pure sample, this variation is decreased to 1 K for Cu-850 sample. Based on the results, the crystallinity improves with the increase of the annealing temperature as a result of the increase in the grain size.

3.2 XRD analyses

Figure 2 shows the X-ray diffraction patterns between 30° and 60° for the bulk MgB_2 superconducting samples annealed at the different temperatures. In this study, all the samples analyzed display the polycrystalline superconducting phase. As seen from the figure, the Cu-850 sample demonstrates the highest peak intensity while the intensity is found to be the smallest for the Cu-0 sample. Additionally, the lattice parameters a and c are calculated using the least-square method through d value and (h k l) planes for hexagonal unit cell structure. The lattice constants are shown in Table 1. The largest lattice cell, a and c, is obtained for

the Cu-850 sample. In addition, the broadening nature of the XRD peaks provides that the particle sizes inferred from the Scherrer–Warren equation are within the nanometer scale [5–7]. According to the equation, in broadening region the average size of a crystal can be described by the following equation:

$$d = \frac{0.941\lambda}{B\cos\theta_B} \tag{1}$$

where d is the thickness of the crystal, k the wavelength, B the full-width half-maximum (FWHM) of the Bragg peak corrected using the corresponding peak in micron-sized powder, and θ_B is the Bragg angle. Moreover,

$$B^2 = B_m^2 - B_s^2 \tag{2}$$

where B_s is the half-width of the standard material in radians. The grain size of the undiffused sample is calculated to be 55 nm (minimum value) whereas that of Cu-850 sample is obtained to be about 74 nm. Based on the calculations, the grain size of the samples studied increases dramatically with the increase of the annealing temperature up to 850 °C (Table 1).

3.3 SEM Analyses

The surface morphology of the MgB_2 material produced is studied by scanning electron microscopy (SEM) images. Figure 3 illustrates the surface micrographs of the undiffused and Cu-850 sample. As can be seen from the figure, the surface morphology of the Cu-diffused sample is denser and smoother while the pure sample has higher porosity. Moreover, the former has larger average crystallite size, better crystallinity and grain connectivity. According to the results of the SEM investigations, the surface morphology, crystallinity and grain size of the Cu-diffused samples improve with the increase of the diffusion-annealing temperature.

3.4 Mechanical Properties and Modeling

In order to understand the effect of Cu diffusion on mechanical properties of the samples produced in this study, the microhardness measurements are performed under different applied loads (0.245–2.940 N) and the load-dependent values are calculated using the following equation [8]:

$$H_V = 1854.4\left(\frac{F}{d^2}\right) \tag{3}$$

where H_V (GPa) is the Vickers hardness, F (N) the applied load, and d (μm) the diagonal length of the indentation. Figure 4 reveals the change in load-dependent microhardness as a function of the applied load. It is obvious from the figure that the microhardness values strongly depend upon the diffusion-annealing temperature and the samples studied show the Indentation Size Effect (*ISE*). The

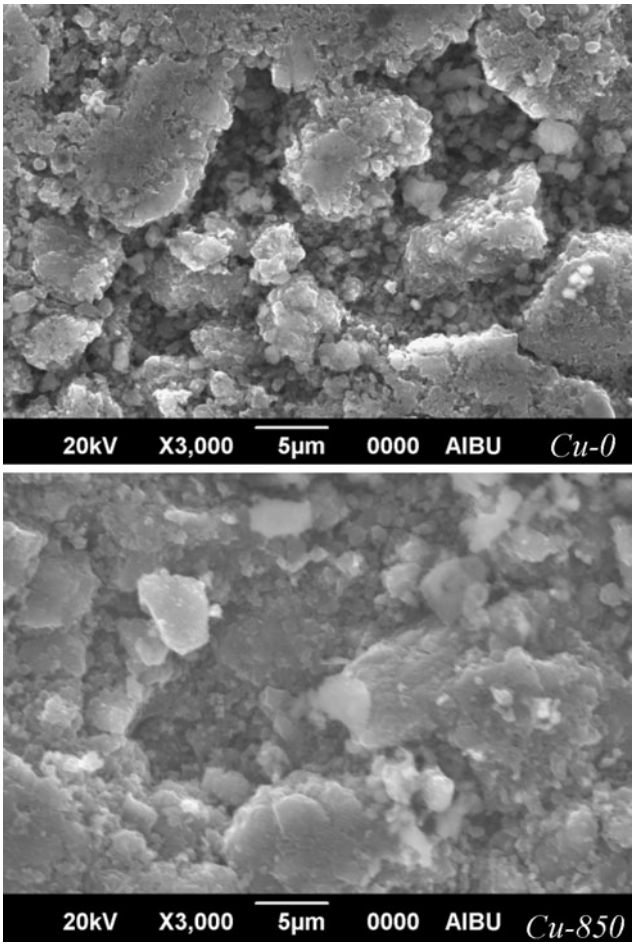

Fig. 3 SEM micrographs Cu-0 and Cu-850 samples

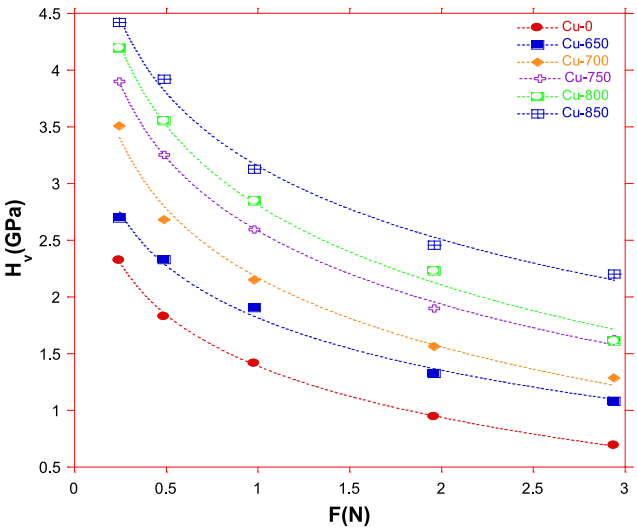

Fig. 4 Variation of load-dependent microhardness H_V with the applied load F

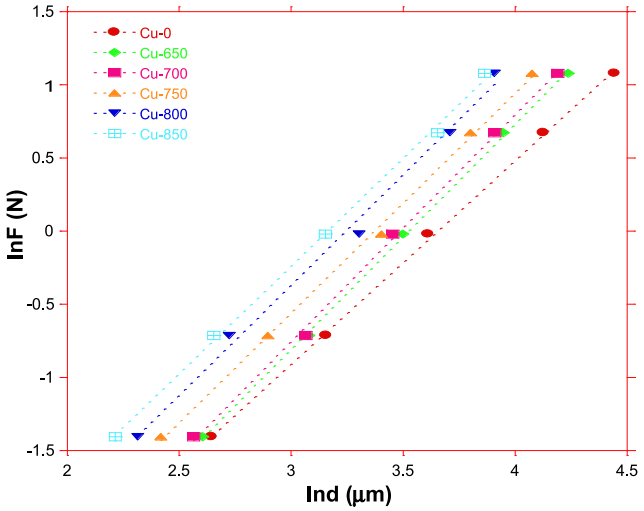

Fig. 5 Variation of the applied load ln F with the diagonal ln d for the samples

H_V values increase rapidly as the applied load increases up to 2 N, beyond which the curves shift to the saturation (plateau) region, confirming the weak grain boundaries, impurity phases and irregular grain orientation distribution [9]. As is known from the literature, different models are forwarded to explore the ISE behavior. In this paper, Meyer's law, Hays–Kendall approach (HK), proportional sample resistance (PSR), modified proportional sample resistance (MPSR), and elastic/plastic deformation (EPD) models are used to analyze microhardness results.

3.4.1 Meyer's Law

Meyer's law gives the relationship between indentation load (F) and the resulting indentation size (d) [10]:

$$F = Ad^n \tag{4}$$

where n is the Meyer number obtained from the fitted curves of the experimental data. The slope of the ln F–ln d graph gives n and the vertical intercept is A. The values of ln A and n obtained from Fig. 5 are listed in Table 2. In contrast, the change of the n value is randomly found in the samples produced. The value of n is observed to be less than 2 for the samples studied, meaning that the load-dependent displacement is due to the ISE behavior. The linear relation in the graph demonstrates that the Meyer's law is suitable for the calculation of microhardness values using different models.

3.4.2 Proportional Specimen Resistance (PSR) Model

According to many researches, the ISE can be described by the following equation [11, 12]:

$$\frac{F}{d} = W_{\mathrm{PSR}} + A_{1\mathrm{PSR}}d \tag{5}$$

Table 2 Best-fit results of experimental data according to Meyer's law

Samples	Meyer number n	ln A
Cu-0	1.392	−5.08
Cu-650	1.539	−5.42
Cu-700	1.551	−5.40
Cu-750	1.501	−5.06
Cu-800	1.508	−4.89
Cu-850	1.471	−4.65

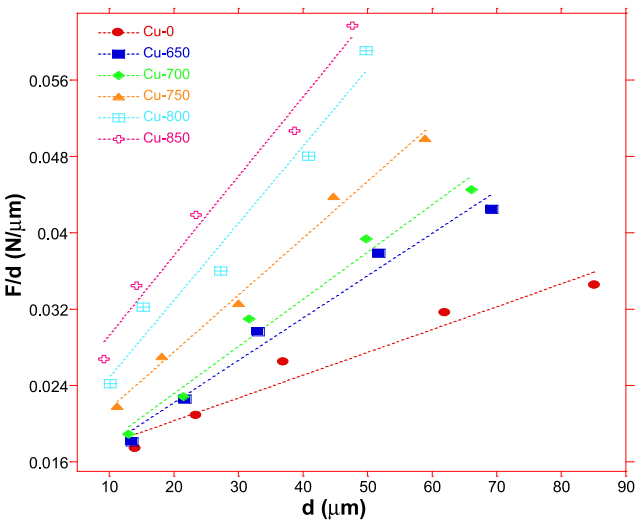

Fig. 6 Plots of F/d vs. d for the samples

The hardness value according to PSR model can be found by equation

$$H_{\mathrm{PSR}} = 1854.4A_{1\mathrm{PSR}} \tag{6}$$

Figure 6 displays the variation of F/d vs. d of the samples. The calculated values of load-independent microhardness values are given in Table 3. The load-independent hardness values increase with the increase of the diffusion-annealing temperature while being lower than the values of the plateau region. Moreover, the calculated load-dependent microhardness values are far from the load-independent microhardness values calculated using PSR model. Therefore, it is obvious that PSR model is not adequate for the determination of the real microhardness value of MgB_2 polycrystals.

3.4.3 Analysis According to Modified PSR (MPSR) Model

MPSR model, being another model to calculate the load-independent microhardness of a material, is proposed to explore the ISE behavior of the material [13]. MPSR model is defined by the following equation:

$$F = W_{\mathrm{MPSR}} + A_{0\mathrm{MPSR}}d + A_{1\mathrm{MPSR}}d^2 \tag{7}$$

Table 3 Best-fit results of experimental data according to PSR model

Samples	W_{PSR} (N)	A_{1PSR} (N/μm) $\times 10^{-4}$	LRC	H_{PSR} (GPa)	H_V (GPa)
Cu-0	0.0015	2.3964	0.9749	0.444	0.751–0.944
Cu-650	0.0132	4.4371	0.9886	0.822	1.136–1.356
Cu-700	0.0133	4.9538	0.9890	0.918	1.248–1.464
Cu-750	0.0155	5.9591	0.9958	1.105	1.570–1.815
Cu-800	0.0167	8.0796	0.9829	1.498	2.202–2.181
Cu-850	0.0209	8.3175	0.9895	1.542	2.402–2.429

Table 4 Best-fit results of experimental data according to MPSR model

Samples	W_{MPRS} (N)	A_{0MPRS} (N/μm)	$A_{1MPRS} \times 10^{-4}$ (N/μm^2)	H_{LMPRS} (GPa)	H_V (GPa)
Cu-0	−0.188	0.0276	1.073	0.199	0.751–0.944
Cu-650	−0.205	0.0278	2.562	0.475	1.136–1.356
Cu-700	−0.191	0.0272	3.072	0.569	1.248–1.464
Cu-750	−0.064	0.0209	5.154	0.955	1.570–1.815
Cu-800	0.138	0.0041	10.027	1.859	2.202–2.181
Cu-850	0.139	0.0060	11.464	2.125	2.402–2.429

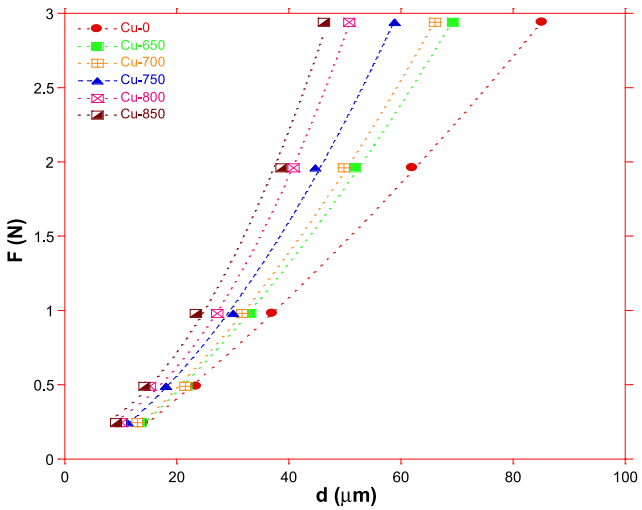

Fig. 7 Variation of the applied load with the indentation diagonal length for the samples

The values of W_{MPSR}, A_{0MPRS} and A_{1MPRS} are obtained from F–d graph as shown in Fig. 7, and the associated load-independent microhardness values are given in Table 4. The load-independent microhardness value due to MPSR model can be calculated by the following equation:

$$H_{MPSR} = 1854.4 A_{1MPRS} \tag{8}$$

As can be seen from Table 4, for the Cu-850 sample the load-independent microhardness value (2.125 GPa) calculated using MPSR model is still lower than the hardness in the plateau region ($H_V = 2.402$–2.429 GPa). This behavior is also observed for all the samples (Cu-0, Cu-650, Cu-700, Cu-750 and Cu-800) in this work. Another important point obtained from the table is that the H_{MPSR} calculated values increase with the increase of the diffusion-annealing temperature.

3.4.4 Analysis According to Elastic/Plastic Deformation (EPD) Model

The dependence of indentation size on the applied load is computed by the following equation [14, 15]:

$$F = A_2(d_e + d_p)^2 \tag{9}$$

where A_2 is a constant, and elastic deformation d_e is related to plastic deformation d_p. Figure 8 demonstrates the applied load dependence of the indentation diagonals investigated using d_p vs. $F^{1/2}$ plots. H_{EPD}, A_2 and d_e values estimated from Fig. 8 are also depicted in Table 5. Additionally, the load-independent microhardness values are calculated by the equation

$$H_{EPD} = 1854.4 A_2 \tag{10}$$

It is seen that the values of load-independent microhardness (H_{EPD}) of the samples increase with the increase of the annealing temperature, similarly to the case for Meyer's, PSR and MPSR models. It is apparent from Table 5 that the value of d_e is positive for all the samples. It means for this range of the applied loads the elastic deformation is observed along with the plastic deformation. Elastic relaxation is present for all the samples. The presence of elastic deformation along with the plastic deformation explains the ISE behavior for our samples.

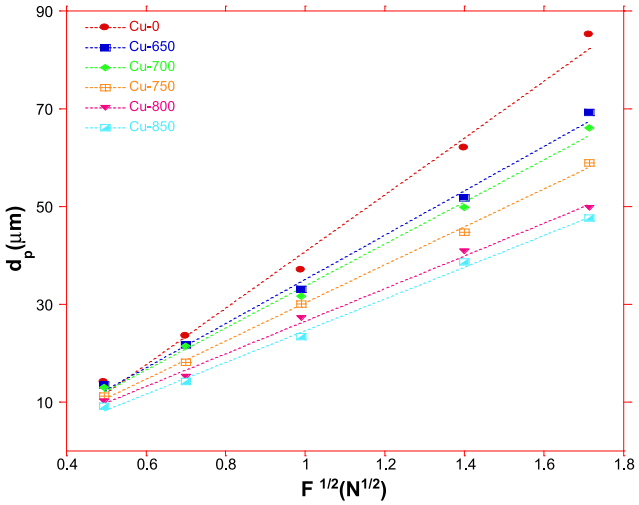

Fig. 8 Plots of diagonal length vs. square root of the applied loads for the samples

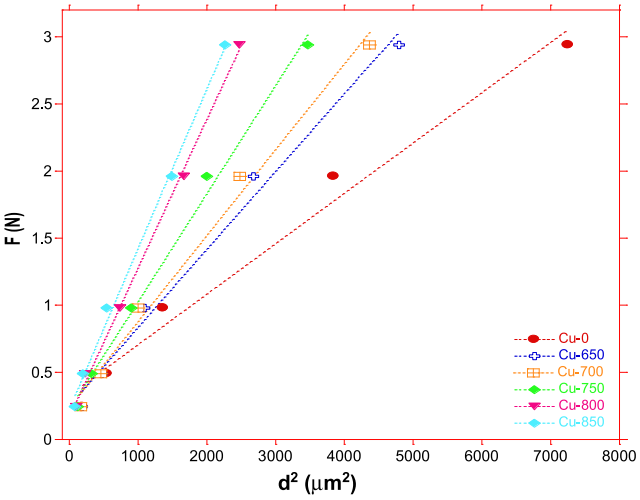

Fig. 9 Applied load vs. the square of the impression length for the samples

Table 5 Best-fit results of experimental data according to EPD model

Samples	H_{EPD} (GPa)	d_e (μm)	LRC	H_V (GPa)
Cu-0	0.551	0.301	0.99566	0.751–0.944
Cu-650	0.904	0.227	0.99768	1.136–1.356
Cu-700	1.001	0.217	0.99787	1.248–1.464
Cu-750	1.224	0.223	0.99916	1.570–1.815
Cu-800	1.660	0.206	0.99814	2.202–2.181
Cu-850	1.756	0.243	0.99845	2.402–2.429

3.4.5 Analysis Using Hays–Kendall Approach

To investigate the ISE behavior, Hays and Kendall (HK) showed that, to produce an indentation, there exist minimum levels of the applied test load (W_{HK}). As is well known, when the n value in the Meyer law is equal to 2, a new formula called Kick's law can be used [16]:

$$F = A_0 d^2 \tag{11}$$

where A_0 is a constant related to the geometry of the indenter tip and tested material of the samples produced. Hays and Kendall proposed that the experimentally measured indentation size is proportional to an effective load $F_{eff} = F - W_{HK}$ instead of the applied load F [17]. Based on this proposition, Eq. (11) is modified to

$$F - W_{HK} = A_{1HK} d^2 \tag{12}$$

where A_{1HK} presents the load-independent hardness constant. According to the HK model, the load-independent microhardness can be calculated using the following equation:

$$H_{HK} = 1854.4 A_{1HK} \tag{13}$$

Figure 9 demonstrates the plots of F vs. d^2 according to Hays–Kendall approach. A straight line is obtained for all the samples, the slope of the line equals to the constant A_{1HK}, and intercept equals to the W_{HK} which characterizes the resistance pressure of the samples. The data show excellent correspondence with high regression coefficients, confirming that the microindentation data of the Cu-diffused MgB_2 materials are successfully described. The estimated best-fit values of A_{1HK} and W_{HK} are listed in Table 6. The values of W_{HK} are obtained to be positive for all the samples, which means that the applied load is sufficient to create both the elastic and the plastic deformation. The calculated values of W_{HK} are found to vary from 0.328 to 0.157 N. As is known, the minimum load is necessary to initiate permanent deformation. In this study, the minimum load of the Cu-0 sample is higher than that of the Cu-850 sample. On the other hand, the estimated values of W_{HK} are generally found to be larger than the acceptable values [18]. Therefore, the HK approach is not a convenient means to estimate the W_{HK} values of the samples. Another interesting result obtained from Table 6 is that the values of H_{HK} and A_{1HK} increase with the increase of the annealing temperature. Comparison between the true hardness values calculated by HK approach ($H_{HK} = 2.208$ GPa) and the apparent hardness results for the Cu-850 sample in the plateau region ($H_V = 2.402$–2.429 GPa) confirms that the HK approach is the most successful model to describe the microhardness mechanism of the samples studied in this work. This behavior is also observed for the other samples (Cu-0, Cu-650, Cu-700, Cu-750 and Cu-800).

In this study, we use five different models to investigate the micro-indentation data on Cu-diffused bulk MgB_2 samples produced. For comparison, the microhardness results of the PSR, MPSR, EPD models and HK approach

Table 6 Best-fit results of experimental data according to HK model

Samples	A_{1HK} (N) $\times 10^{-4}$	W_{HK} (N)	LRC	H_{HK}	H_V
Cu-0	3.756	0.328	0.9905	0.696	0.751–0.944
Cu-650	5.812	0.251	0.9944	1.077	1.136–1.356
Cu-700	6.397	0.238	0.9951	1.186	1.248–1.464
Cu-750	8.049	0.223	0.9971	1.492	1.570–1.815
Cu-800	11.062	0.168	0.9991	2.051	2.202–2.181
Cu-850	11.910	0.157	0.9980	2.208	2.402–2.429

Table 7 The results of load-dependent Vickers microhardness at the plateau region and load-independent hardness values calculated using PSR, MPSR, EPD models and the HK approach

Samples	H_{PSR} (GPa)	H_{LMPRS} (GPa)	H_{EPD} (GPa)	H_{HK}	H_V (GPa)
Cu-0	0.444	0.199	0.551	0.696	0.751–0.944
Cu-650	0.822	0.475	0.904	1.077	1.136–1.356
Cu-700	0.918	0.569	1.001	1.186	1.248–1.464
Cu-750	1.105	0.955	1.224	1.492	1.570–1.815
Cu-800	1.498	1.859	1.660	2.051	2.202–2.181
Cu-850	1.542	2.125	1.756	2.208	2.402–2.429

are given along with Vickers microhardness values of the samples in the plateau region in Table 7. The table shows that the Vickers microhardness values increase with the increase of the diffusion-annealing temperature up to 850 °C. The similar behavior is observed for all the compared models.

To sum up, the load-independent microhardness values calculated by HK approach give closer results to the ones in the plateau region than compared to the PSR, MPSR and EPD models. It is argued that the load-independent microhardness values are expected to be close to those in the plateau region [19, 20]. Therefore, the Hays–Kendall approach is the most suitable method to investigate the mechanical properties of the Cu-diffused bulk MgB_2 superconductors.

4 Conclusion

In the present work, we examined the effect of the diffusion-annealing temperature on the microstructural, electrical, physical, superconducting and mechanical properties of the Cu-diffused bulk MgB_2 superconductor materials with the aid of the dc resistivity, SEM, XRD and Vickers microhardness measurements. Moreover, the results of the microhardness measurements are examined using different models such as Meyer's law, PSR, MPRS, EPD, and Hays–Kendall approach. The results obtained reveal that the electrical, structural, physical, mechanical and superconducting properties of the samples depend strongly on the diffusion-annealing temperature and the major conclusions to be obtained from this work are the following:

- The critical temperature values are obtained to increase systematically with the increase in the diffusion-annealing temperature. Namely, the T_c^{onset} and T_c^{offset} values are found to be about 39.3 and 38.3 K for the Cu-850 sample whereas the former and the latter for undiffused sample are obtained to be about 38.4 and 36.9 K, respectively, presenting that the variation of ΔT_c decreases with the increase of the diffusion-annealing temperature.
- The XRD examinations reveal that both the peak intensities and the lattice parameters a and c increase monotonously with the increase of the diffusion-annealing temperature.
- According to the SEM investigations, not only do the surface morphology and grain connectivity improve but the crystallite size of the samples also becomes bigger with the increase in the annealing temperature up to 850 °C. The decrease in the crystallite size is favored by means of the grain size calculations of the XRD peaks.
- The Vickers microhardness values obtained improve with the increase of the annealing temperature as a result of the increment in the strength of the bonds between grains, being incompatible with the SEM investigation since the grain connectivity and surface morphology improve and the voids and porosity decrease with the increase in the diffusion-annealing temperature.
- The results of the microhardness measurements are analyzed employing Meyer's law, PSR, MPSR, EDP models and Hays–Kendall approach. Hays–Kendall approach is found to be the best model to examine the mechanical properties of the Cu-diffused bulk MgB_2 superconductors.

References

1. Awad, R., Abou Aly, A.I., Kamal, M., Anas, M.: J. Supercond. Nov. Magn. **24**, 1947–1956 (2011)
2. Ozturk, O., Cetinkara, H.A., Asikuzun, E., Akdogan, M., Yilmazlar, M., Terzioglu, C.: J. Mater. Sci., Mater. Electron. **22**, 1501–1508 (2011)
3. Aydin, H., Cakiroglu, O., Nursoy, M., Terzioglu, C.: Chin. J. Phys. **47**, 192–206 (2009)
4. Terzioglu, C.: J. Alloys Compd. **509**, 87–93 (2011)
5. Dogruer, M., Yildirim, G., Yucel, E., Terzioglu, C.: J. Mater. Sci., Mater. Electron. (2012). doi:10.1007/s10854-012-0689-6
6. Dogruer, M., Gorur, O., Zalaoglu, Y., Ozturk, O., Yildirim, G., Varilci, A., Terzioglu, C.: J. Mater. Sci., Mater. Electron. (2012). doi:10.1007/s10854-012-0755-0
7. Yildirim, G., Varilci, A., Akdogan, M., Terzioglu, C.: J. Mater. Sci., Mater. Electron. **23**, 928–935 (2012)
8. Economy, J., Anderson, R.: Inorg. Chem. **5**, 989–992 (1966)
9. Terzioglu, C., Varilci, A., Belenli, I.: J. Alloys Compd. **478**, 836–841 (2009)
10. Wang, H., Serquis, A., Maiorov, B., Civale, L., Jia, Q.X., Arendt, P.N., Foltyn, S.R., Macmanus-Driscoll, J.L., Zhang, X.: J. Appl. Phys. **100**, 053904 (2006)
11. Li, H., Bradt, R.C.: J. Mater. Sci. **28**, 917–926 (1993)
12. Khalil, S.M.: J. Phys. Chem. Solids **62**, 457–466 (2001)
13. Gong, J., Wu, J., Guan, Z.: J. Eur. Ceram. Soc. **19**, 2625–2631 (1999)
14. Upit, G.P., Varchenya, S.A.: Phys. Status Solidi A **17**, 831–835 (1966)
15. Bull, S.J., Page, T.F., Yoffe, E.H.: Philos. Mag. Lett. **59**, 281–288 (1989)
16. Kolemen, U.: J. Alloys Compd. **425**, 429–435 (2006)
17. Hays, C., Kendall, E.G.: Metallurgy **6**, 275–282 (1973)
18. Nursoy, M., Yilmazlar, M., Terzioglu, C., Belenli, I.: J. Alloys Compd. **459**, 399–406 (2008)
19. Gong, J., Zhao, Z., Guan, Z., Mıao, H.: J. Eur. Ceram. Soc. **20**, 1895–1900 (2000)
20. Peng, Z., Gong, J., Mıao, H.: J. Eur. Ceram. Soc. **24**, 2193–2201 (2004)